FOREX Publication
Open Access | Rapid and quality publishing

International Journal of
Electrical and Electronics Research (IJEER)
Research Article | Volume 12, Issue 4 | Pages 1151-1162 | e-ISSN: 2347-470X

Optimizing Real-Time Scheduling for Post Islanding Energy Management Using African Vulture Optimization Algorithm on Hybrid Microgrids Environment

Ramya Madamaneri[1*] and Dr Devaraju T[2]

[1]*Research Scholar, Mohan Babu University, India; mramya2020@gmail.com*
[2]*Professor in EEE, Mohan Babu University, India; devaraj@vidyanikethan.edu*

***Correspondence:** Ramya Madamaneri; *mramya2020@gmail.com*

ABSTRACT- Microgrids (MG) are small-scale energy systems that use distributed energy storage and sources. Hybrid microgrids are transforming energy management by incorporating various energy resources like wind, solar, and battery storage. Effective scheduling of this resource is vital to minimize the costs and maximize energy autonomy. Advanced scheduling algorithm optimizes the operation of hybrid microgrids, which dynamically adjusts the energy consumption and generation to satisfy the demand while ensuring power balancing. This scheduling strategy has been instrumental in improving the sustainability and resilience of MGS, which paves the way for an environmentally friendly and more reliable energy future. They can operate on islanded or grid-connected modes. The optimization of hybrid MG scheduling is paramount in the field of post-island management to ensure effective energy sustainability and distribution. Using metaheuristic approaches like simulated annealing or genetic algorithms allows the finetuning of scheduling parameters to increase energy utilization while reducing environmental impact and costs. Therefore, the study presents a Real-Time Scheduling for Post Islanding Energy Management using African Vulture Optimization Algorithm (RTSPIEM-AVOA) in Hybrid microgrid environment. The RTSPIEM-AVOA approach is utilized to improve its functioning by determining the most efficient scheduling of the installed generation unit. The AVOA can handle complex optimization issues while avoiding local optima solutions because of the balance among the exploitation and exploration stages. A microturbine (MT) system, battery storage, a fuel cell (FC), photovoltaic (PV), and wind turbine (WT) make up the suggested MG system. This work looks at three scenarios: PV and WT operating at normal generation, PV and WT operating at their maximum power, and WT operating at its rated power. Consider the two objective functions of minimizing pollutant emissions and reducing operational costs. According to the experimental results, the RTSPIEM-AVOA technique outperforms other models in microgrid scheduling by efficiently optimizing it to satisfy the community's changing needs while transitioning to a greener and more sustainable energy future.

Keywords: Microgrids; African Vulture Optimization Algorithm; Renewable Energy Source; Microturbine; Photovoltaic.

ARTICLE INFORMATION

Author(s): Ramya Madamaneri and Dr Devaraju T;
Received: 26/07/2024; **Accepted**: 24/09/2024; **Published**: 15/10/2024;
e-ISSN: 2347-470X;
Paper Id: IJEER 2607-23;
Citation: 10.37391/ijeer.120405
Webpage-link:
https://ijeer.forexjournal.co.in/archive/volume-12/ijeer-120405.html

Publisher's Note: FOREX Publication stays neutral with regard to Jurisdictional claims in Published maps and institutional affiliations.

1. INTRODUCTION

Recently, power systems have witnessed a transformative leap, from hierarchical evolution to structural modification [1]. Renewable energy sources (RES) and non-renewable energy sources are interconnected to establish a distributing system that operates more effectively, economically, and reliably, helping to resist global warming. In addition, the advancement of RES plays a major role in finding a solution to the problem of energy sources in remote and rural regions. A microgrid (MG) system comprises energy storage devices, distributed generators (DGs), power conversion units, one or multiple loads, etc., which ensures heat demand and/or local electricity is met [2]. MGs can be operated in grid-connected mode or can provide off-grid areas with electricity. Even though off-grid MGs show great promise, particularly in inaccessible locations, they encounter significant energy scheduling and control problems [3]. Likewise, the realization of safe and economical operation of an MG is a real challenge for researcher workers since the RES is subjected to specific limits, and the capacity of this system is limited. An MG contains Energy storage units, critical/non-critical loads and multiple generation units [4]. The point of common coupling (PCC) is used for connecting MG to the utility grid (UG). The distributed generation unit has PEI connection to obtain control protection, and metering objectives along with plug-in features, whether in islanded mode or grid-connected. The MG can supply the surplus power to the utility if the MG is connected to UG [5]. In case of failure or disturbance in the UG, The MG can change its operation mode from grid-connected to islanded mode. Under any circumstance, the critical load is first supplied by the MG. Then, MG central controller (MGCC) controls the operation together with local controllers (LC) [6]. The sustainable development and system performance have been dramatically increased by

FOREX Publication
Open Access | Rapid and quality publishing
International Journal of Electrical and Electronics Research (IJEER)
Research Article | Volume 12, Issue 4 | Pages 1151-1162 | e-ISSN: 2347-470X

the energy management system (EMS) in MG and effective coordination of Distributed Energy Resources (DERs).

One of the key features of MG system is that it works on different islanded and grid-tied modes [7]. The increase of renewable source-based DG continues with the increasingly widespread use of MGs. The deployment ability of MG can offer various benefits, such as efficiency improvement, risk and emission reductions, cost reduction, and increase in the incorporation of DG into the grid [8]. However, the MG still faces certain difficulties. For instance, they require control strategies and innovative management since traditional strategies cannot often respond to the dynamic behaviors of MG. Thus, there is a need for appropriate control strategy to ensure smooth power switching in MGs, especially in islanding conditions [9]. Also, the control system should improve the PQ of MGs and control the frequency variation, voltage variation, and phase angles to retain them within the desirable limit. Islanding detection is vital to avoid PQ problems and hazards [10]. The controller can maintain a stable frequency and voltage to transmit renewable energy to the consumer once the MG is disconnected from the UG. The key supervisory controller in the MG system is EMS.

In a hybrid microgrid (MG) scenario, this work uses the African Vulture Optimization Algorithm (AVOA) for real-time scheduling in post-islanding energy management. Through the identification of the installed generation unit's ideal schedule, the RTSPIEM-AVOA approach is utilized to enhance its performance. By balancing the exploration and exploitation phases, the AVOA effectively avoids local optima and addresses challenging optimization problems. A fuel cell (FC), solar (PV) panels, wind turbines (WT), battery storage, and a microturbine (MT) system are all integrated into the suggested MG system. Consider the two objective functions which are minimizing the pollutant emission and mitigating the operating cost. Based on the results of the examination, the RTSPIEM-AVOA technique outperforms other models in terms of performance and successfully optimizes MG scheduling to meet community requirements as they change and move the energy sector closer to being more sustainable and greener.

2. LITERATURE REVIEW

Huy et al. [11] introduce a SL approach for real-world power scheduling of isolated MG. The presented method consists of three stages: Firstly, the mixed-integer linear programming (MILP) algorithm is introduced for the optimum power scheduling problems of isolated MG to reduce the cost of operations. Next, an SL strategy is established for learning and mimicking optimum ESS charging or discharging decisions by the dense ResNet (ResNetD) training on the expert database. Zia et al. [12] introduce a two-step supervisory EMS for optimum operation of PV/Wind/Tidal MG with one-time transmission. The initial phase schedules the optimum energy supply from all the energy sources thus improving the effectiveness. The second phase updates the decision strategy by analyzing the demand profile and scheduled generation to ensure efficient utilization. In [13], suggested a novel approach for ESS scheduling. The probabilistic model is introduced for the network parameters and expressed as MILP problem to consider the uncertainty related to the multi objective scheduling problems. The non-dominated sorting TLBO (NSTLBO) technique is utilized for resolving the problems of MO.

Abdelghany et al. [14] developed a model predictive control (MPC) technique for managing the wind–solar MG in the grid-connected and islanded modes. The system participates in the real-time and daily markets, represented by the time scale. Hence, a low-layer control (LLC) and a high-layer control (HLC) are introduced. The sporadic features of RES and the variation in load demands are deliberated by suggesting the controller based on the stochastic MPC method. In [15], proposed an EMS technique. An algorithm for two-step hierarchical optimization is used in the suggested method. MMG (multi-Microgrid) optimization comes after MG (Microgrid) optimization in the first step. MG resources are utilized to address any residual deficit. The presented technique is expressed as a non-linear complicated optimization problem that is more efficiently managed by the metaheuristic approaches. An effective hybrid approach is suggested by Roy et al. [16] for the Energy Management System (EMS) of a microgrid (MG) running in grid-tied mode. This method combines Artificial Neural Networks (ANN) and the Hybrid Whale Optimization (HWO) algorithm. The proposed model designs the best balance of MG based on the load demand prediction. Furthermore, the two techniques for MG energy management were utilized. The first technique focuses on the different RES programming. The second technique is to balance the PF and reduce the prediction error effects based on the rules drawn from the scheduled power reference.

To manage the distribution of energy in response to demand unpredictability and renewable energy sources (RES), a hierarchical online Energy Management System (HEMS) was presented in [17]. In order to provide seasonal energy shifting and on-site battery stack management, the HEMS deployed a hydrogen energy storage unit based on electrolyze-fuel cells. It is possible to decouple the fuzzy logic (FL)-based controller and enable the HEMS to make decisions in real time by employing operating frequency. For evaluation purposes, a Local Energy Estimation Model (LEEM) was also created expressly. A method for energy balancing was provided by Hartani et al. [18], which used a Mamdani 50 rule-based FL-EMS to control and monitor State-of-Charge (SoC) recovery.

3. SYSTEM MODELING OF MGS

This section introduces a typical isolated MG system [19]. Subsequent sections will explore detailed discussions on the output power of distributed generation. A classic MG model containing RES generation, HESS, and sequence of loads. Distributed power generation mostly consists of two components: fossil energy generation using diesel engines and renewable energy sources using solar and wind power. As HESS, a battery and supercapacitor are used. Approaching the HESS within MG can resolve this issue that 2 energy storages can be limited by the response speed and energy density utilized individually. It is effectual measure to enhance the stability and

FOREX Publication
Open Access | Rapid and quality publishing
International Journal of Electrical and Electronics Research (IJEER)
Research Article | Volume 12, Issue 4 | Pages 1151-1162 | e-ISSN: 2347-470X

economy of MG. At last, controllable and uncontrollable loads are the 2 kinds of loads within distributed power systems.

Distributed Energy Modeling

(1) RES System

Photovoltaic Power Generation

The resultant power of PV system is defined as:

$$P_{PV} = P_{PV,STC} \times \frac{R}{R_{STC}} \times \left(1 - \beta \times (T_a - T_r)\right) \quad (1)$$

$$T_a = T_{amb} + \frac{R}{R_{STC}} \times (T_{NOC} - 20) \quad (2)$$

Wind Power Generation Modelling

In place of a WT system, the power transformation equation of transforming to WT outcome in the wind power is written as:

$$P_W = \frac{1}{2}\rho\pi R_w^2 V_w^3 C_P \quad (3)$$

$$C_P = f(\theta, \lambda) \quad (4)$$

The blade-tip speed ratio is demonstrated by the following expression:

$$\lambda = \frac{w_w R}{V_w} \quad (5)$$

The carbon emission is extremely low (approximately 20 g/kWh) designed for the PV system. Additionally, the carbon emission is associated with wind power systems are significantly lower. So, the carbon emissions from distributed energy generation can be ignored depending on the previous analysis.

(2) Energy Storage System

In power systems, energy storage units exist in two procedures. The former is energy-type storage; e.g., lithium batteries, lead-acid batteries, and sodium-sulfur batteries. The latter is power type; the superconducting magnetic energy storage, super-capacitors, and flywheel energy storage are generally utilized power-type units. The structure of HESS meets various levels of demand to reduce peak demand from the distributed energy system and enhance the value of renewable energy penetration.

Battery Modelling

The energy obtainable for discharge and charging that battery offers as:

$$E_b = C_b U_b \gamma \mu_b \times 10^{-3} \quad (6)$$

Generally, the battery voltage is constant, and its functioning current is usually measured at around 0. $1C$ (C defines the capacity) A, thus the resultant power of battery is written as:

$$P_b = C_b U_b \times 10^{-4} \quad (7)$$

Super-capacitor Modelling

The electric power that is generated by the ultra-capacitor from all the charges and discharges is defined as:

$$E_c = 0.5 \times C_c \eta_a (U_{c,\max}^2 - U_{c,\min}^2)/(3.6 \times 10^6) \quad (8)$$

$$P_c = U_{c,\max} I_{c,\max} \quad (9)$$

Then, the HESS (batteries and super-capacitors) could not use fossil fuels, and their emissions CO_2 are disregarded.

(3) Load System

Upon analyzing the distribution of loads within the MG, the presented loads are considered into 4 portions. The 1st type of controllable load is given below:

$$P_{j,t} = X_{j,t} P_j \forall j \in J \quad (10)$$

$$\sum_{t \in T} X_{j,t} = H_j \forall j \in J \quad (11)$$

$$\begin{Bmatrix} X_{j,t} \in (0,1) | & t \in \Omega_j \\ X_{j,t} = 0 | & t \in \Omega_j \end{Bmatrix} \forall j \in J \quad (12)$$

The 2nd type of controllable load is expressed as:

$$P_{k,t} = X_{k,t} P_k \forall k \in K \quad (13)$$

$$X_{k,t} + X_{k,t+1} + \cdots + X_{k,t+q_k^2} \geq a_k \quad (14)$$

$$\forall k \in K, \forall t = 1,2,\cdots, t_{\max} - b_k$$

$$\begin{Bmatrix} X_{k,t} \in (0,1) | t \in \Omega_k \\ X_{k,t} = 0 | t \in \Omega_k \end{Bmatrix} \forall k \in K \quad (15)$$

The 3rd type of controllable load is demonstrated as:

$$P_{l,t} = X_{l,t} P_l \forall l \in L \quad (16)$$

$$X_{l,t} P_{l,t,\min} \leq X_{l,t} P_l \leq X_{l,t} P_{l,t,\max} \quad (17)$$

$$E_{l,\min} \leq \sum_{t \in T} (P_{l,t} \Delta t) \leq E_{l,\max} \quad (18)$$

$$\begin{Bmatrix} X_{l,t}^{III} \in (0,1) | t \in \Omega_l \\ X_{l,t}^{III} = 0 | t \in \Omega_l \end{Bmatrix} \forall l \in L \quad (19)$$

4. THE PROPOSED MODEL

In this study, we have presented an RTSPIEM-AVOA on hybrid MGs environment. To improve operational efficiency, the best schedule for the installed generation units is determined using the RTSPIEM-AVOA approach. *Figure 1* represents the working flow of RTSPIEM-AVOA approach.

4.1. Design of AVOA

The AVOA becomes a flexible and easy-to-use metaheuristic technique influenced by eating and positioning behaviors of African vultures. [20] AVOA is extensively utilized through numerous optimization fields, providing versatility for modifications and applications that cause optimum outcomes. Vultures in the wild show different behaviors dependent upon their physical abilities, dividing into two groups. They are proficient at avoiding tricks because of their greedy starvation

FOREX Publication
Open Access | Rapid and quality publishing
International Journal of Electrical and Electronics Research (IJEER)
Research Article | Volume 12, Issue 4 | Pages 1151-1162 | e-ISSN: 2347-470X

and insistence on hunting for food. The two stronger and more effective vultures have been regarded as the more strong and optimum outcomes. The next subsections will discuss the AVOA method's general steps. *Figure 2* represents the steps involved in AVOA.

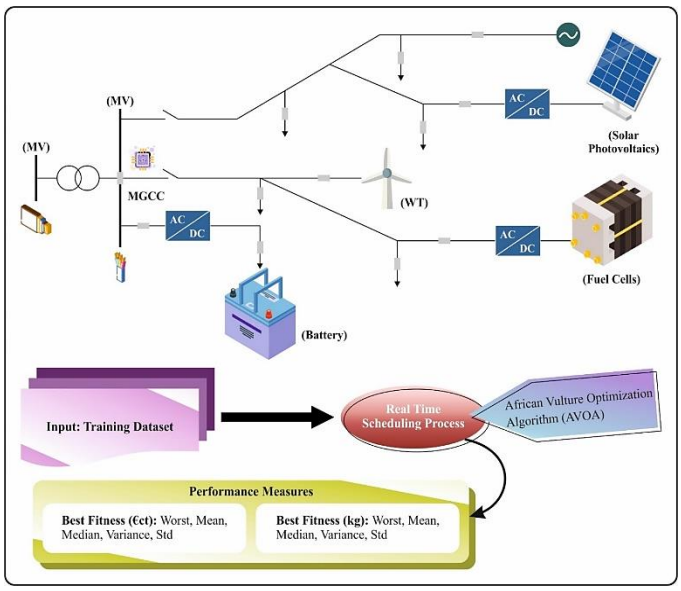

Figure 1. Working flow of RTSPIEM-AVOA system

The fitness of every solution is calculated after the development of the initial population, and the highest execution outcome is chosen as the fittest vulture from 1st group, represented as BV_1, whereas the 2nd best outcome will be recognized as the fittest vulture from 2nd group, represented as BV_2. The resultant rule can be given below,

$$R(k) = \begin{cases} BV_1 & if \quad p_i = B_1 \\ BV_2 & if \quad p_i = B_2 \end{cases} \tag{20}$$

Now, B_1 and B_2 describes measured values that previous to the search process. Such factors are values ranging from 0 to 1, and $B_1 + B_2 = 1$. Also, the choice of major best solutions will be accomplished by applying a roulette wheel mechanism as represented below:

$$p_i = F_i / (\sum_{i=1}^{n} F_i) \tag{21}$$

The regular food-searching of vultures and improved durability later eating permit them to travel more in their search for food. They lose energy while they are starving, making it difficult for them for higher distances in food search. In these conditions, they often search for food near robust vultures and turn out to be aggressive in hunger. This mathematical model for this behavior will be demonstrated as given below:

$$t = h \times \left(\sin^w \left(\frac{\pi}{2} \times \frac{k}{k_{\max}} \right) + \cos \left(\frac{\pi}{2} \times \frac{k}{k_{\max}} \right) - 1 \right) \tag{22}$$

$$F = (2 \times r_{v1} + 1) \times S \times \left(1 - \frac{k}{k_{\max}} \right) + t. \tag{23}$$

From Eq. (22) and (23), F characterizes the satisfaction level of vultures, $S \in [1, 1]$, $h \in [2, 2]$ and $r_{v1} \in [0,1]$ describes random values. Once the value of S is under zero, it specifies that the vulture at the condition of hunger, if improves from S - zero specifies satisfaction. In the AVOA method, the value F performs a key role in determining if the method arrives at exploration or exploitation stages. Particularly, when $|F| > 1$, the method starts the exploration stage and when $|F| \leq 1$, it initiates the exploitation stage.

At the exploration stage, the vultures utilize the dual approaches to examine random fields and choice of the approach should be directed by a predetermined factor named $P_1 \in [0,1]$ that could be defined previous to the initiation of the search process. To decide which approach to employ in the "randP1" exploration stage, a random number can be produced with the range of 0 to 1, represented as r_{p1}. When $P_1 \geq r_{p1}$ parameter, and after the subsequent rule will be utilized.

$$\begin{cases} VP(k+1) = R(k) - D(k) \times F \\ D(k) = |X \times R(k) - VP(k)| \end{cases} \tag{24}$$

Here F refers to the satiation rate of the vulture, $VP(k)$ and $VP(k+1)$ characterize the vulture's vector positions at the existing and following iterations correspondingly, $R(i)$ signifies top vultures, and X point out the arbitrary motion in protecting the food from alternative vultures. The random movement is varied with every iteration and can be estimated by applying the mathematical equation $X = 2 \times \text{rand}$, the value rand $\in [0,1]$ refers to the random number to be performed as the strengthening coefficient of X. If $P_1 < r_{p1}$, after the next mathematical formula will be utilized in *equation (25)*

$$VP(k+1) = R(k) - F + r_{v2} \times \left((ub - lb) \times r_{v3} + lb \right) \tag{25}$$

Now, $r_{v2}, r_{v3} \in [0,1]$ describes randomized numbers, and "lb" and "ub" denote the lower and upper boundaries, respectively. In the exploitation phase, there are two major stages such as stage 1 and stage 2. The AVOA transformation to stage 1 if $|F| \in [0.5,1)$. It comprises 2 approaches named rotating flight and siege-flight schemes that will be explained in detailed manner:

The serious competition for achievement of foods among weaker and stronger vultures will be imitated via the next rule:

$$\begin{cases} VP(k+1) = D(k) \times (F + r_{v4}) - d(t) \\ d(t) = R(k) - VP(k) \end{cases} \tag{26}$$

Whereas $r4 \in [0,1]$ defines a random value. The mathematical formula offers the distance among the fittest vultures.

The rotational competition will be demonstrated arithmetically in a spiral movement. By applying the method, a mathematical model encompassing each vulture and the two best vultures will be generated. The movement will be represented as follows:

FOREX Publication
Open Access | Rapid and quality publishing
International Journal of Electrical and Electronics Research (IJEER)
Research Article | Volume 12, Issue 4 | Pages 1151-1162 | e-ISSN: 2347-470X

$$\begin{cases} S_1 = R(k) \times \left(\frac{r_{v5} \times VP(k)}{2\pi}\right) \times cos(P(k)) \\ S_2 = R(k) \times \left(\frac{r_{v6} \times VP(k)}{2\pi}\right) \times cos(P(k)) \\ VP(k+1) = R(i) - (S_1 + S_2) \end{cases} \quad (27)$$

where $r_{v5}, r_{v6} \in [0,1]$ describes random values.
To choose the approach, a $P_2 \in [0,1]$ was presented earlier in the search operation initialization. The r_{p2} has been created at the beginning of this stage. According to r_{p2} and P_2, the choice of scheme must be modeled as given below.

$$VP(k+1) = \begin{cases} (26) & if \quad P_2 \geq r_{p2} \\ (27) & if \quad P_2 < r_{p2} \end{cases} \quad (28)$$

The AVOA evolutions to stage 2 if $|F| < 0.5$. This stage comprises two methods such as "Congregation of diverse varieties of vultures near the food sources" and "Destructive competition for food". These approaches will be more discussed as follows:
During this phase of AVOA, the movement of vultures for collecting nearby food sources should be detected. While vultures have been starved, there will rarely be aggressive competition for food that could be caused by various categories of vultures for collecting about a single food source that will be mathematical representation is given below,

$$\begin{cases} A_1 = BV_1(k) - \frac{BV_1(k) \times VP(k)}{BV_1(k) - VP(k)^2} \times F \\ A_2 = BV_2(k) - \frac{BV_2(k) \times VP(k)}{BV_2(k) - VP(k)^2} \times F \\ VP(k+1) = \frac{A_1 + A_2}{2} \end{cases} \quad (29)$$

Now, BV_1 and BV_2 defines the fittest vulture in the 1st and 2nd groups correspondingly.

During this phase of AVOA, the prominent vultures become weak and starving, therefore incapable of challenging alternative vultures for food. Whereas alternative vultures are starved become destructive and begin to change into the top vultures. Their movements will be represented as given below,

$$VP(k+1) = R(k) - |d(t)| \times F \times Levy(d) \quad (30)$$

Here $d(t)$ characterizes the distance between the vulture and fittest vultures. The application of the Levy fight improves the effectiveness.

To choose the approach, a $P_3 \in [0,1]$ must be presented previously the search arises. A random number, r_{p3}, could be produced at the arrival of this stage. As stated by r_{p3} and P_3, the approach selection can be mathematically formed as given below

$$VP(k+1) = \begin{cases} (26) & if \quad P_3 \geq r_{p3} \\ (27) & if \quad P_3 < r_{p3.} \end{cases} \quad (31)$$

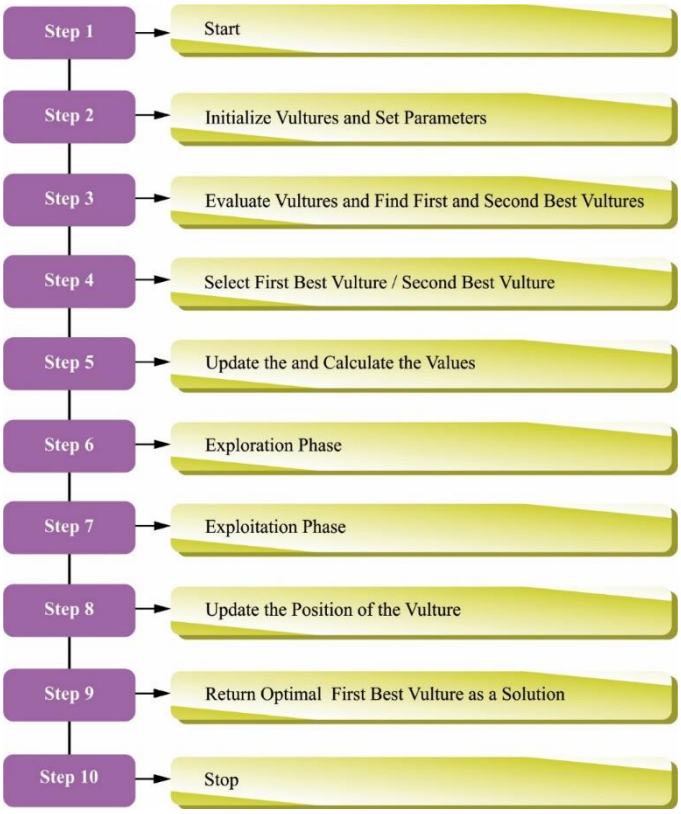

Figure 2. Steps involved in AVOA

4.2. Modeling of Real-Time Scheduling using RTSPIEM-AVOA technique

In the RTSPIEM-AVOA technique, consider two objective functions which are minimizing the pollutant emission and mitigating the operating cost. The MG designing strategies belong to mechanism of the economical dispatch procedure where the load is disseminated in optimum method among the creating units connected within MG so that the complete operating cost can be diminished [21]. Conversely, to enhance the efficiency of MG, it is vital to alleviate the pollutant emission in the DGs. Thus, author maintains either operational cost or pollutant emission as a target. The operational cost of MG signifies the startup cost, shutdown cost, and fuel cost, it is expressed as:

$$F_1(x) = \sum_{h=1}^{24} (C_r(h) + C_b(h) + C_g(h)) \quad (32)$$

Whereas, $C_r(h)$, $C_b(h)$, and $C_g(h)$ denotes the operational cost of creating units, batteries, and grid at hour h, correspondingly. The rate of $C_r(h)$ has been computed utilizing *equation (33)*.

$$C_r(h) = C_{PV}(h) + C_{WT}(h) + C_{MT}(h) + C_{FC}(h) \quad (33)$$

In which, $C_{PV}(h)$, $C_{WT}(h)$, $C_{MT}(h)$, and $C_{FC}(h)$ implies the costs of PV, WT, MT, and FC correspondingly, it is computed as:

$$C_{PV}(h) = u_{PV}(h)P_{PV}(h)B_{PV}(h) + S_{PV}(h)|u_{PV}(h) - u_{PV}(h-1)| \quad (34)$$

FOREX Publication
Open Access | Rapid and quality publishing
International Journal of Electrical and Electronics Research (IJEER)
Research Article | Volume 12, Issue 4 | Pages 1151-1162 | e-ISSN: 2347-470X

$$C_{WT}(h) = u_{WT}(h)P_{WT}(h)B_{WT}(h) + S_{WT}(h) \times |u_{WT}(h) - u_{WT}(h-1)| \quad (35)$$

$$C_{MT}(h) = u_{MT}(h)P_{MT}(h)B_{MT}(h) + S_{MT}(h)|u_{MT}(h) - u_{MT}(h-1)| \quad (36)$$

$$C_{FC}(h) = u_{FC}(h)P_{FC}(h)B_{FC}(h) + S_{FC}(h)|u_{FC}(h) - u_{FC}(h-1)| \quad (37)$$

Whereas, $u_{PV}(h)$, $u_{WT}(h)$, $u_{MT}(h)$, and $u_{FC}(h)$ denotes the conditions of PV, WT, MT, and FC at hour h correspondingly, $P_{PV}(h)$, $P_{WT}(h)$, $P_{MT}(h)$, and $P_{FC}(h)$ stands for the generated power in the earlier state modules, $B_{PV}(h)$, $B_{WT}(h)$, $B_{MT}(h)$, and $B_{FC}(h)$ implies the bids of MG modules, $S(h)$ and $S(h-1)$ demonstrate the startup and shutdown costs at h and $h-1$ hours correspondingly.

The battery and grid costs are measured as:

$$C_b(h) = u_b(h)P_b(h)B_b(h) + S_b(h)|u_b(h) - u_b(h-1)| \quad (38)$$

$$C_g(h) = P_g(h)B_g(h) \quad (39)$$

In which, $u_b(h)$ denotes the battery position, $P_b(h)$ and $P_g(h)$ represents the battery and grid powers at hour h, $B_b(h)$ and $B_g(h)$ defines the battery and grid bids. The power outputs of the generating units and their operational states, stated as follows, are the variables taken into account in this problem:

$$x = \left[P_{PV}, P_{WT}, P_{MT}, P_{FC}, P_b, P_g, u_{PV}, u_{WT}, u_{MT}, u_{FC}, u_b\right] \quad (40)$$

Grid is the primary source of pollutant emission from the created MG and any DGs such as FCs, and batteries. This leads to higher levels of pollutant emissions that contain nitrogen dioxide (NO_x), carbon dioxide (CO_2), and sulfur dioxide (SO_2). The pollutant emission is defined as:

$$F_2(x) = \sum_{h=1}^{24}\left[\sum_{i=1}^{N_g}\left(u_i(h)P_{Gi}(h)E_{Gi}(h)\right) + \sum_{j=1}^{N_s}\left(u_j(h)P_{Si}(h)E_{Si}(h)\right) + P_g(h)E_g(h)\right] \quad (41)$$

Whereas, $E_{Gi}(h)$, $E_{Si}(h)$, and $E_g(h)$ signifies the entire emitted pollutants in the generation units, storage devices, and grid, correspondingly, N_g implies the count of generating units, and N_s defines the count of storage devices.

Constraints on the optimization issue include power generation boundaries, load balancing, ramp limits of renewable energy sources (RESs), and battery charging and discharging circumstances. At any moment, the power generated must be adequate to fulfill the load demand, which is indicated by the load balance constraint, expressed as follows:

$$\sum_{i=1}^{N_g} P_{Gi}(h) + \sum_{j=1}^{N_s} P_{bj}(h) + P_g(h) = \sum_{e=1}^{N,\Sigma} P_L(h) \quad (42)$$

In which, N_k defines the count of load points and $P_L(h)$ indicates the load power at h hour.

The second limitation defines the ramp values of RESs, it can be enhancing or reducing within generation, it is written as:

$$R_{di}\Delta T \le \left(P_i(h) - P_i(h-1)\right) < R_{ui}\Delta T \quad (43)$$

In which, R_{di} and R_{ui} refers to the ramp-up and down of i^{th} DG, correspondingly, and ΔT stands for the time step. The generated power in all the devices installed in MG must accomplish the following *equation (44)*.

$$P_{Gi,min}(h) \le P_{Gi}(h) < P_{Gi,max}(h) P_{bi,min}(h) \le P_{bi}(h) < P_{bi,max}(h) \quad (44)$$

$$P_{g,min}(h) \le P_g(h) < P_{g,max}(h)$$

Whereas, max stands for the maximal boundary but min signifies the minimal boundary. The constrictions allocated to the battery function are vital to avoid damage,

$$E_{b,\min} \le E_b(h) < E_{b,max} \quad (45)$$

$$P_{ch}(h) \le P_{ch^{rated}}, P_{disch}(h) \le P_{disch^{rated}} \quad (46)$$

In which, $E_{b,\min}$ and $E_{b,max}$ implies the battery's minimal and maximal stored energies correspondingly, $P_{ch^{roted}}$ and $P_{disch^{roted}}$ stands for the battery's maximal charging and discharging powers, correspondingly. The energy stored from the battery at h hour is measured as:

$$E_b(h) = E_b(h-1) + \xi_{ch}P_{ch}(h)\Delta T - \frac{1}{\xi_{disch}}P_{disch}(h)\Delta T \quad (47)$$

Whereas, ξ_{ch} and ξ_{disch} refers to the battery charging and discharging efficacies, correspondingly.

5. EXPERIMENTAL VALIDATION

In this section, the simulation analysis of the RTSPIEM-AVOA method is tested using different scenarios, as listed below.

- Scenario1: Normal operation of PV and WT
- Scenario2: Operation of WT at rated power
- Scenario3: Operation of PV and WT at rated powers

5.1 Dataset

- The MAR regional climate model is used by the University of Liège's Laboratory of Climatology to provide weather forecasts, which include air temperature and solar radiation, every 15 minutes.
- In the MiRIS microgrid, PV generation and consumption were tracked with a 5-second resolution.
- Our forecaster generated weather-based projections for PV generation and consumption with a 15-minute resolution, which were used in the study.

With a resolution of 15 minutes, the weather forecasts are multi-output predictions covering a 24-hour period [21]. They are produced utilizing a one-week learning set, rolling periodically. Every six hours, the model is updated, and the learning set is modified correspondingly.

FOREX Publication
Open Access | Rapid and quality publishing
International Journal of Electrical and Electronics Research (IJEER)
Research Article | Volume 12, Issue 4 | Pages 1151-1162 | e-ISSN: 2347-470X

This means that a PV and consumption prediction of 96 values is generated every quarter (one for each quarter of the next 24 hours). More information about the MiRIS microgrid, located at the John Cockerill Group's international headquarters in Seraing, Belgium, can be found at https://johncockerill.com/fr/energy/stockage-denergie/.

5.2 Implementation Tool

MATLAB and General Algebraic Modeling Software (GAMS) were used to do the simulation. The African Vulture Optimization Algorithm (AVOA) in MATLAB was used to calculate the energy purchase and sale prices inside the cluster layer of microgrids as well as the energy sales pricing for each microgrid to consumers. These costs were inputs used to solve the GAMS optimization issue.

Table 1 reports the overall total operation cost (TOC) outcomes of the RTSPIEM-AVOA method with existing models in Scenario1 [22]. *Fig. 3* inspects the best fitness (BF) results of the RTSPIEM-AVOA method with existing technique. The outcomes highlighted that the TDO, ARO, and CHIO models have shown worse performance with least BF of 111.2540€ct, 111.3790€ct, and 115.3970€ct, correspondingly. At the same time, the MRFO and DAOA techniques have shown slightly decreased BF of 113.2300€ct and 112.4660€ct correspondingly. Meanwhile, the HBA has managed to obtain certainly reduced BF of 103.4130€ct. However, the RTSPIEM-AVOA technique reaches optimal performance with minimal BF of 90.4130€ct.

Figure 4 examines the elapsed time (ET) outcomes of the RTSPIEM-AVOA method with existing models. The results emphasized that the TDO, ARO, and CHIO techniques have shown worse performance with minimum ET of 1144.6930s, 840.6840s, and 1250.6400s, correspondingly. Simultaneously, the MRFO and DAOA methods have shown slightly reduced ET of 1575.9800s and 784.5030s correspondingly. Meanwhile, the HBA has managed to attain certainly reduced ET of 614.0530s. However, the RTSPIEM-AVOA method obtains optimum performance with least ET of 581.0530s.

Table 1. TOC analysis of RTSPIEM-AVOA technique with existing models on Scenario1

Minimizing the TOC in scenario1							
Parameter	**TDO**	**ARO**	**CHIO**	**MRFO**	**DAOA**	**HBA**	**RTSPIEM-AVOA**
Best fitness (€ct)	111.2540	111.3790	115.3970	113.2300	112.4660	103.4130	90.4130
Worst (€ct)	993.6950	732.0380	831.4630	551.3440	872.8470	224.0200	211.0200
Mean (€ct)	118.7370	125.6960	160.6660	131.1310	218.3060	108.8550	89.8550
Median (€ct)	111.7890	113.5760	126.6990	119.9720	180.5160	108.4130	90.4130
Variance (€ct)	41.9755	42.0878	42.4442	43.0513	42.8693	4.8492	3.0100
Std (€ct)	6.4789	6.4875	6.5149	6.5614	6.5475	2.2021	1.9800
Elapsed time (s)	1144.6930	840.6840	1250.6400	1575.9800	784.5030	614.0530	581.0530
Minimizing the pollutant emission in scenario1							
Best fitness (kg)	182.0810	182.3590	275.5860	183.1260	582.5390	182.0740	56.0740
Worst (kg)	873.3610	631.5600	892.0540	557.4120	951.0020	575.9690	485.9690
Mean (kg)	185.7870	195.4290	313.6610	197.3650	650.6400	185.7230	50.7230
Median (kg)	182.1350	182.8690	290.5860	184.7770	626.0950	182.1240	38.1240
Variance (kg)	8.8562	8.8339	8.4013	8.7153	54.6283	0.0052	0.0032
Std Std (€ct)	2.9759	2.9722	2.8985	2.9522	7.39109	0.0718	0.0049
Elapsed time (s)	1144.6900	840.6840	1250.6400	1575.9800	784.5030	614.0530	522.0530

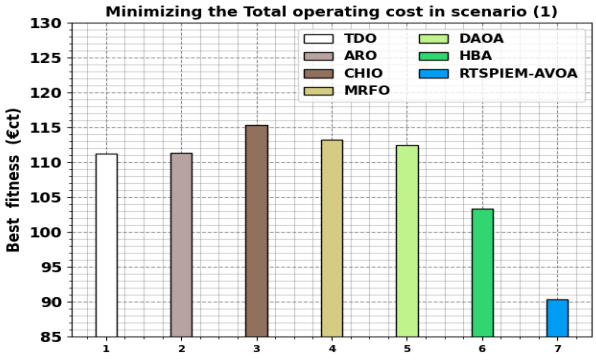

Figure 3. BF analysis of RTSPIEM-AVOA method on scenario1

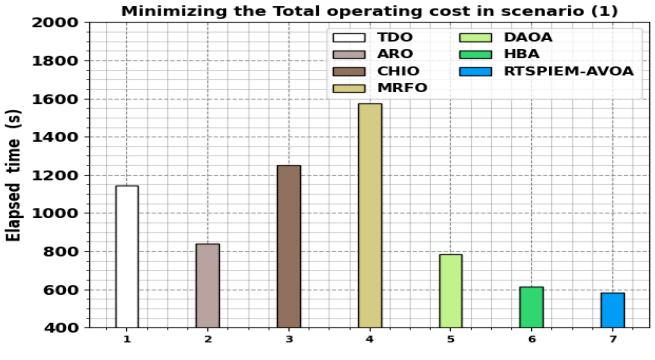

Figure 4. ET analysis of RTSPIEM-AVOA method on Scenario1

FOREX Publication
Open Access | Rapid and quality publishing
International Journal of Electrical and Electronics Research (IJEER)
Research Article | Volume 12, Issue 4 | Pages 1151-1162 | e-ISSN: 2347-470X

Figure 5 shows the emission results of the RTSPIEM-AVOA method with existing systems under Scenario1. According to the findings, the DAOA approach performed less well than optimal at maximum emission levels. Followed by, the TDO, ARO, CHIO, MRFO, and HBA models have resulted in somewhat reduced emission levels. Nevertheless, the RTSPIEM-AVOA technique shows better performance over other models with the lowest emission levels.

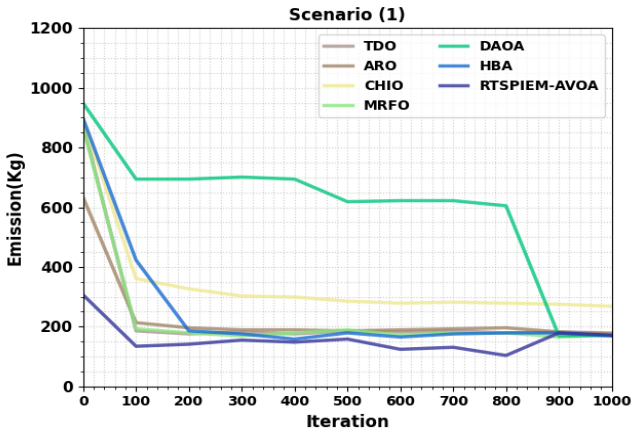

Figure 5. Emission analysis of RTSPIEM-AVOA approach on Scenario1

Table 2 examines the overall TOC outcomes of the RTSPIEM-AVOA approach with existing methods in Scenario2. *Figure 6* reviews the BF outcomes of the RTSPIEM-AVOA method with existing techniques. The results emphasized that the TDO, ARO, and CHIO approaches have shown worse performance with minimum BF of 55.582€ct, 55.724€ct, and 60.165€ct, correspondingly. Simultaneously, the MRFO and DAOA techniques have shown slightly decreased BF of 57.764€ct and 56.676€ct correspondingly. Meanwhile, the HBA has managed to attain certainly decreased BF of 55.580€ct. But the RTSPIEM-AVOA method obtains optimum performance with least BF of 48.580€ct.

Figure 7 inspects the ET results of the RTSPIEM-AVOA method with existing techniques. The results highlighted that the TDO, ARO, and CHIO approaches have revealed worse performance with minimum ET of 1144.693s, 840.684s, and 1250.640s, correspondingly. Simultaneously, the MRFO and DAOA techniques have shown slightly decreased ET of 1575.980s and 784.503s correspondingly. Meanwhile, the HBA has managed to attain certainly decreased ET of 614.053s. However, the RTSPIEM-AVOA method obtains optimum performance with least ET of 557.053s.

Table 2. TOC analysis of RTSPIEM-AVOA technique with existing models on Scenario2

Minimizing the TOC in scenario2							
Parameter	**TDO**	**ARO**	**CHIO**	**MRFO**	**DAOA**	**HBA**	**RTSPIEM-AVOA**
Best fitness (€ct)	55.582	55.724	60.165	57.764	56.676	55.580	48.580
Worst (€ct)	939.290	630.610	933.870	434.750	535.890	435.650	425.650
Mean (€ct)	63.146	67.508	97.845	72.105	134.530	60.390	55.390
Median (€ct)	56.291	56.440	67.705	63.149	139.220	55.580	50.580
Variance (€ct)	18.301	18.417	19.928	19.567	18.681	18.300	10.300
Std (€ct)	4.278	4.291	4.464	4.423	4.322	4.278	2.722
Elapsed time (s)	1144.693	840.684	1250.640	1575.980	784.503	614.053	557.053
Minimizing the pollutant emission in scenario (2)							
Best fitness (kg)	145.944	145.945	159.634	146.171	324.958	137.008	30.008
Worst (kg)	752.899	600.313	658.708	550.711	459.245	708.795	615.795
Mean (kg)	148.770	157.656	211.261	158.956	356.798	141.685	32.685
Median (kg)	145.946	146.073	187.347	147.267	358.102	137.650	42.650
Variance (kg)	0.604	0.604	0.983	0.599	12.163	0.001	0.000
Std (€ct)	0.777	0.777	0.991	0.774	3.488	0.025	0.015
Elapsed time (s)	1069.830	790.374	1507.500	1176.130	651.459	607.052	512.052

FOREX Publication
Open Access | Rapid and quality publishing
International Journal of Electrical and Electronics Research (IJEER)
Research Article | Volume 12, Issue 4 | Pages 1151-1162 | e-ISSN: 2347-470X

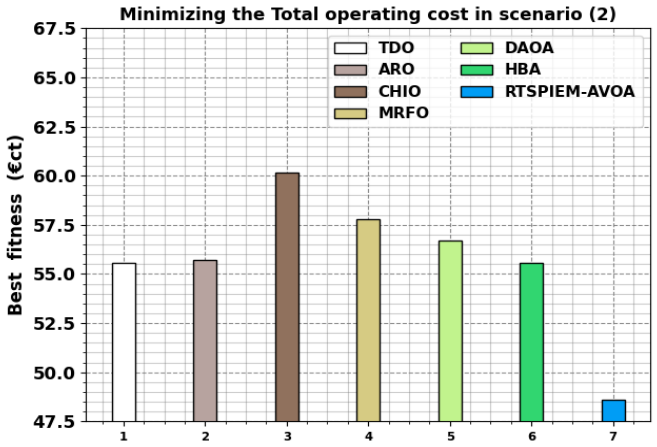

Figure 6. BF analysis of RTSPIEM-AVOA method on Scenario2

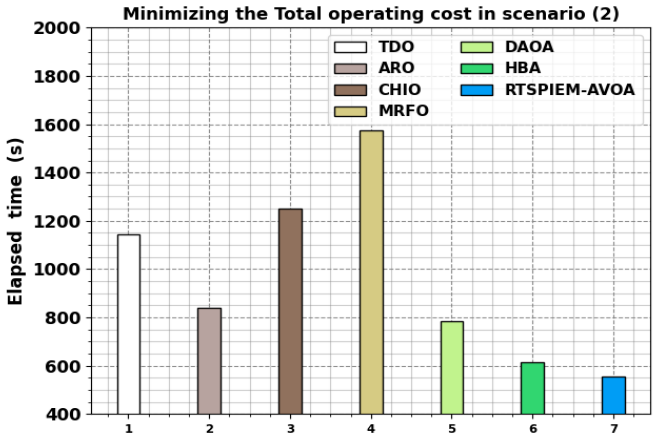

Figure 7. ET analysis of RTSPIEM-AVOA technique on Scenario2

Figure 8 shows the emission outcomes of the RTSPIEM-AVOA method with existing approaches under Scenario2. The outcome shows that the DAOA method has demonstrated poor performance with maximum emission levels. Followed by, the TDO, ARO, CHIO, MRFO, and HBA approaches have resulted in somewhat reduced emission levels. Nonetheless, the RTSPIEM-AVOA method illustrates the best performance over other techniques with minimum emission levels.

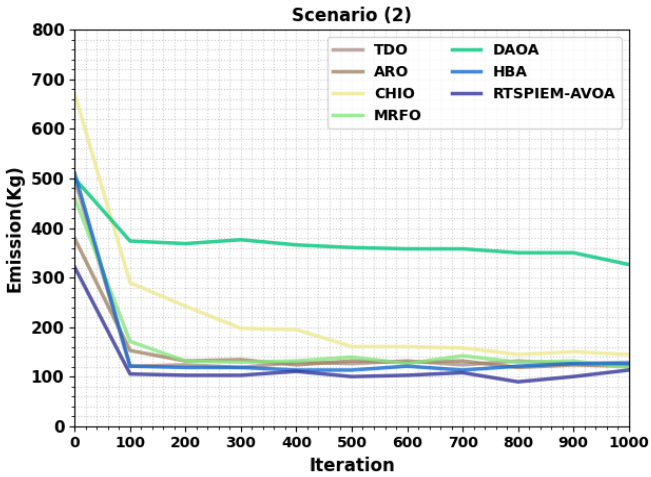

Figure 8. Emission analysis of RTSPIEM-AVOA technique in Scenario2

Table 3 reports the overall TOC outcomes of the RTSPIEM-AVOA method with existing techniques in Scenario3. *Figure 9* examines the BF outcomes of the RTSPIEM-AVOA method with existing techniques. The outcomes emphasized that the TDO, ARO, and CHIO approaches have shown worse performance with minimum BF of 89.069€ct, 89.066€ct, and 108.673€ct, correspondingly. Simultaneously, the MRFO and DAOA methods have shown slightly reduced BF of 91.822€ct and 122.796€ct correspondingly. Meanwhile, the HBA has managed to attain certainly decreased BF of 87.890€ct. However, the RTSPIEM-AVOA method obtains best performance with least BF of 33.890€ct.

Table 3. TOC analysis of RTSPIEM-AVOA technique with existing models on Scenario3

Minimizing the Total operating cost in scenario (3)							
Parameter	**TDO**	**ARO**	**CHIO**	**MRFO**	**DAOA**	**HBA**	**RTSPIEM-AVOA**
Best fitness (€ct)	89.069	89.066	108.673	91.822	122.796	87.890	33.890
Worst (€ct)	738.853	588.108	829.766	506.106	741.180	529.737	484.737
Mean (€ct)	101.297	100.793	143.768	112.734	222.409	95.403	40.403
Median (€ct)	91.783	91.256	113.314	100.052	218.107	87.971	31.971
Variance (€ct)	35.103	35.607	38.499	36.783	52.976	4.816	3.084
Std (€ct)	5.925	5.967	6.205	6.065	7.278	2.195	1.906
Elapsed time (s)	1707.730	1464.074	2155.500	1892.530	1224.859	1199.552	1095.352
Minimizing the pollutant emission in scenario (3)							
Best fitness (kg)	134.988	135.479	173.532	139.118	458.675	134.805	96.805
Worst (kg)	624.170	467.957	636.160	413.689	647.019	452.889	421.889
Mean (kg)	137.663	143.881	210.747	148.178	527.224	136.880	85.880
Median (kg)	135.369	135.955	191.142	140.098	531.177	134.839	74.839
Variance (kg)	0.014	0.022	1.316	0.011	29.901	0.016	0.010
Std (kg)	0.120	0.148	1.147	0.105	5.468	0.126	0.104
Elapsed time (s)	1044.730	764.074	1468.500	1140.530	620.859	575.552	476.352

FOREX Publication
Open Access | Rapid and quality publishing
International Journal of Electrical and Electronics Research (IJEER)
Research Article | Volume 12, Issue 4 | Pages 1151-1162 | e-ISSN: 2347-470X

Figure 10 scrutinizes the ET outcomes of the RTSPIEM-AVOA method with existing techniques. The outcomes emphasized that the TDO, ARO, and CHIO approaches have shown worse performance with minimum ET of 1707.730s, 1464.074s, and 2155.500s, correspondingly. Simultaneously, the MRFO and DAOA methods have shown slightly reduced ET of 1892.530s and 1224.859s correspondingly. Meanwhile, the HBA has managed to attain certainly decreased ET of 1199.552s. However, the RTSPIEM-AVOA method obtains optimum performance with least ET of 1095.352s.

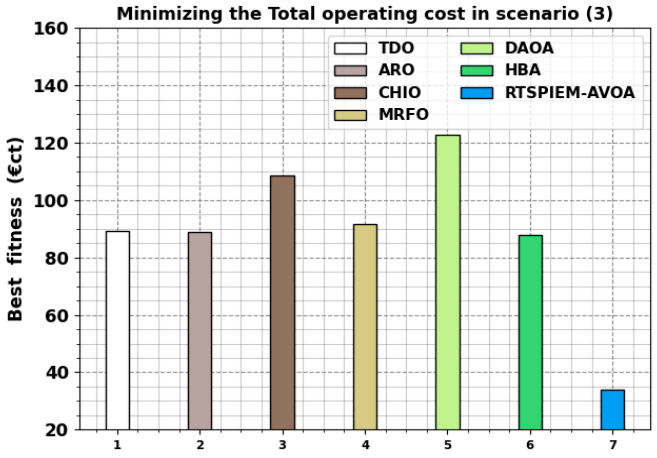

Figure 9. BF analysis of RTSPIEM-AVOA technique on Scenario3

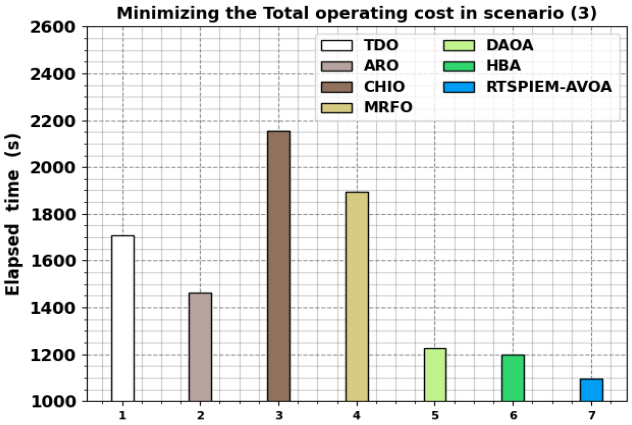

Figure 10. ET analysis of RTSPIEM-AVOA technique on Scenario3

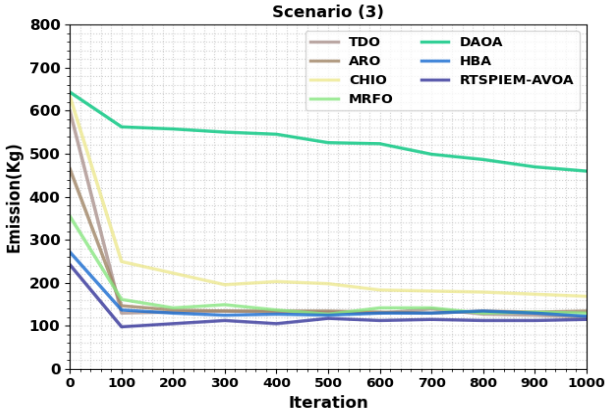

Figure 11. Emission analysis of RTSPIEM-AVOA technique on Scenario3

Figure 11 demonstrates the emission outcomes of the RTSPIEM-AVOA method with existing approaches under Scenario3. The results show that the DAOA approach had unsatisfactory performance, resulting in the greatest levels of emissions. Followed by, the TDO, ARO, CHIO, MRFO, and HBA techniques have resulted in somewhat decreased emission levels. Nonetheless, the RTSPIEM-AVOA method is superior to other techniques with minimum emission levels. Therefore, the RTSPIEM-AVOA technique can be applied for enhanced scheduling in hybrid MG environment.

Table 4. Comparison of cost estimation and voltage convergence with traditional methods

Reference	Wind system ($/kW)	Solar Panel ($/kW)	Fcs ($/kW)	Electrolyzer ($/kW)	Total or Total Number of Iterations	Total cost after Assessment $	Voltage Convergence	Power quality improvement
[23]	-	60	2	45	-	-	No	No
[24]	5	5	5	30	1408s	-	No	No
[25]	200	360	150	-	3500s	-	No	No
[26]	900	770	907	439	200 iterations	2.44×10^7 to 2.33×10^7		
Proposed	700	800	900	400	100 iterations	2.99×10^7 to 2.173×10^7	Yes	Yes

Table 4 demonstrates unequivocally that the method used lowers the cost of a microgrid system from $24.4 million to $22.9 million while improving power quality over 100 iterations.

Table 5. Computational complexity Analysis for proposed RTSPIEM-AVOA model

Models	Computational complexity
TDO	1.191
ARO	1.204
CHIO	1.232
MRFO	1.278
DAOA	1.156
HBA	1.123
RTSPIEM-AVOA	1.029

FOREX Publication
Open Access | Rapid and quality publishing
International Journal of Electrical and Electronics Research (IJEER)
Research Article | Volume 12, Issue 4 | Pages 1151-1162 | e-ISSN: 2347-470X

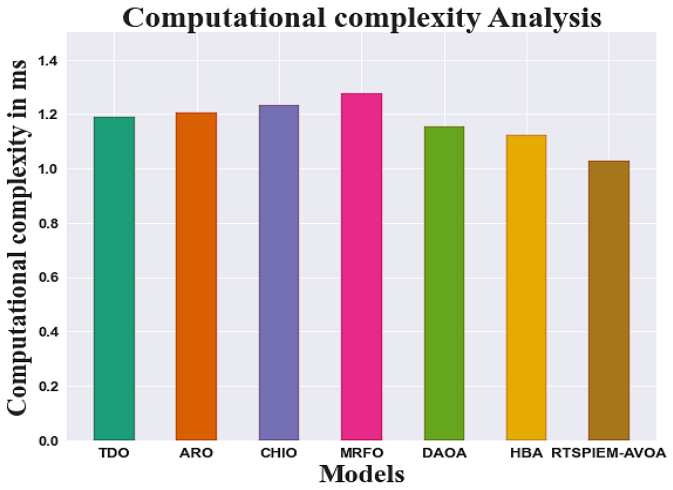

Figure 12. Computational complexity Analysis for proposed RTSPIEM-AVOA model

In *table 5* and *figure 12*, the computational complexity of the proposed RTSPIEM-AVOA method is associated to that of existing methods. The data clearly displays that the RTSPIEM-AVOA method outperformed all other approaches. The recommended RTSPIEM-AVOA method, for instance, took only 1.029ms to compute, whereas other present approaches such as TDO, ARO, CHIO, MRFO, DADO, HBA and HBA have taken 1.191ms, 1.204ms, 1.232ms, 7.198ms, 1.278ms, 1.156ms and 1.123ms, respectively.

5.2 Discussion

The integration of the African Vulture Optimization Algorithm (AVOA) for optimizing real-time scheduling in post-islanding energy management represents a significant advancement in hybrid microgrid environments. The research demonstrates that AVOA effectively addresses the complex challenges of energy distribution and management following an islanding event, where traditional centralized control methods may falter. The algorithm's bio-inspired mechanisms, mimicking the foraging behavior of African vultures, facilitate efficient exploration of the solution space, enabling the identification of optimal energy management strategies that balance supply and demand while minimizing operational costs. This adaptive approach is particularly crucial in hybrid microgrids, where diverse energy sources, including renewable and conventional, must be seamlessly integrated. The outcomes also highlight the essential function that flexible scheduling systems with the ability to swiftly adapt to changing real-time situations perform. By leveraging AVOA, the proposed method not only enhances the responsiveness of the microgrid system but also contributes to its resilience against potential disruptions, thereby ensuring reliable energy supply during critical periods.

6. CONCLUSION

In this study, we have presented an RTSPIEM-AVOA on hybrid MGs environment. The RTSPIEM-AVOA method is used to improve its operation by detecting the optimum scheduling of the installed generation unit. The AVOA balances the exploitation and exploration stages to effectively deal with complex optimization problems and prevent local optima. The proposed MG includes FC, PV, WT, battery storage, and MT systems. Three scenarios are examined in this study: photovoltaic (PV) and wind turbine (WT) systems operating normally, WT systems operating at maximum power generation, and both PV and WT systems operating at their rated capacity. We take into account two target functions: lowering operational costs and decreasing pollutant emissions. Based on experimental results, the RTSPIEM-AVOA technique works better than previous models and efficiently optimizes microgrid scheduling to meet community demands as they change and to support a more environmentally conscious and sustainable energy future.

REFERENCES

[1] W.S. Ho, S. Macchietto, J.S. Lim, H. Hashim, Z.A. Muis, W.H. Liu, Optimal scheduling of energy storage for renewable energy distributed energy generation system, Renew Sustain Energy Rev 58 (2016) 1100–110.

[2] Raghav, L. Phani, Seshu Kumar, R., Koteswara Raju, D., Singh, Arvind R., 2021. Optimal energy management of microgrids using quantum teaching learning-based algorithm. IEEE Trans. Smart Grid 12 (6), 4834–4842.

[3] Li, N., Su, Z., Jerbi, H., Abbassi, R., Latifi, M., Furukawa, N., 2021. Energy management and optimized operation of renewable sources and electric vehicles based on microgrid using hybrid gravitational search and pattern search algorithm. Sustainable Cities Soc. 75, 103279.

[4] X. Kong, L. Bai, Q. Hu, F. Li, C. Wang, Day-ahead optimal scheduling method for grid-connected microgrid based on energy storage control strategy, J. Mod. Power Syst. Clean Energy 4 (4) (2016) 648–658.

[5] Adefarati, T., Bansal, R.C., Bettayeb, M., Naidoo, R., 2021. Optimal energy management of a PV-WTG-BSS-DG microgrid system. Energy 217, 119358.

[6] S. Rajamand, M. Shafie-khah, J.P.S. Catalao, ˜ Energy storage systems implementation and photovoltaic output prediction for cost minimization of a Microgrid, Electr. Power Syst. Res. 202 (Jan. 2022), 107596.

[7] Kim, H.J., Kim, M.K., Lee, J.W., 2021. A two-stage stochastic p-robust optimal energy trading management in microgrid operation considering uncertainty with hybrid demand response. Int. J. Electr. Power Energy Syst. 124, 106422.

[8] Y.R. Lee, H.J. Kim, M.K. Kim, Optimal operation scheduling considering cycle aging of battery energy storage systems on stochastic unit commitments in microgrids, Energies 14 (2) (2021).

[9] H. Takano, R. Hayashi, H. Asano, T. Goda, Optimal sizing of battery energy storage systems considering cooperative operation with microgrid components, Energies 14 (21) (2021) 1–13.

[10] Ghasemi, A. and Enayatzare, M., 2018. Optimal energy management of a renewable-based isolated microgrid with pumped-storage unit and demand response. Renewable energy, 123, pp.460-474.

[11] Huy, T.H.B., Le, T.D., Van Phu, P., Park, S. and Kim, D., 2024. Real-time power scheduling for an isolated microgrid with renewable energy and energy storage system via a supervised-learning-based strategy. Journal of Energy Storage, 88, p.111506.

[12] Zia, M.F., Nasir, M., Elbouchikhi, E., Benbouzid, M., Vasquez, J.C. and Guerrero, J.M., 2022. Energy management system for a hybrid PV-Wind-Tidal-Battery-based islanded DC microgrid: Modeling and experimental validation. Renewable and Sustainable Energy Reviews, 159, p.112093.

[13] Rahmani, E., Mohammadi, S., Zadehbagheri, M. and Kiani, M., 2023. Probabilistic reliability management of energy storage systems in connected/islanding microgrids with renewable energy. Electric Power Systems Research, 214, p.108891.

International Journal of
Electrical and Electronics Research (IJEER)
Research Article | Volume 12, Issue 4 | Pages 1151-1162 | e-ISSN: 2347-470X

[14] Abdelghany, M.B., Al-Durra, A., Daming, Z. and Gao, F., 2024. Optimal multi-layer economical schedule for coordinated multiple mode operation of wind–solar microgrids with hybrid energy storage systems. Journal of Power Sources, 591, p.233844.

[15] Mahmoud, I., Hasanien, H.M., Turky, R.A. and Omran, W.A., 2023. Energy management system for islanded multi-microgrids using a two-stage optimization scheme based on political optimizer. IET Renewable Power Generation, 17(7), pp.1713-1730.

[16] Roy, K., Mandal, K.K. and Mandal, A.C., 2022. Energy management system of microgrids in grid-tied mode: A hybrid approach. Energy Sources, Part A: Recovery, Utilization, and Environmental Effects, pp.1-23.

[17] Wu, J., Li, S., Fu, A., Cvetković, M., Palensky, P., Vasquez, J.C. and Guerrero, J.M., 2024. Hierarchical online energy management for residential microgrids with Hybrid hydrogen–electricity Storage System. Applied Energy, 363, p.123020.

[18] Hartani, M.A., Rezk, H., Benhammou, A., Hamouda, M., Abdelkhalek, O., Mekhilef, S. and Olabi, A.G., 2023. Proposed frequency decoupling-based fuzzy logic control for power allocation and state-of-charge recovery of hybrid energy storage systems adopting multi-level energy management for multi-DC-microgrids. Energy, 278, p.127703.

[19] Chen, H., Gao, L., Zhang, Z. and Li, H., 2021. Optimal energy management strategy for an islanded microgrid with hybrid energy storage. Journal of Electrical Engineering & Technology, 16, pp.1313-1325.

[20] B.T. Geetha, P. Santhosh Kumar, B. Sathya Bama, Chiranjit Dutta, D. Vijendra Babu, Green energy aware and cluster-based communication for future load prediction in IoT, Sustainable Energy Technologies and Assessments, Vol.52,2022,102244, https://doi.org/10.1016/j.seta.2022.102244

[21] https://www.kaggle.com/datasets/jonathandumas/liege-microgrid-open-data

[22] Perumal SK, Kallimani JS, Ulaganathan S, Bhargava S, Meckanizi S. Controlling energy aware clustering and multihop routing protocol for IoT assisted wireless sensor networks. Concurrency Computat Pract Exper. 2022;e7106. doi: 10.1002/cpe.71.

[23] Paladini, V.; Donateo, T.; de Risi, A.; Laforgia, D. Super-capacitors fuel-cell hybrid electric vehicle optimization and control strategy development. Energy Convers. Manag. 2007, 48, 3001–3008.

[24] Onori, S.; Serrao, L.; Rizzoni, G. Adaptive Equivalent Consumption Minimization Strategy for Hybrid Electric Vehicles. 2010. Available online: https://api.semanticscholar.org/CorpusID:12583370 (accessed on 25 January 2011).

[25] Zhang, W.; Li, J.; Xu, L.; Ouyang, M. Optimization for a fuel cell/battery/capacity tram with equivalent consumption minimization strategy. Energy Convers. Manag. 2017, 134, 59–69.

[26] adehFard, H.; Tooryan, F.; Collins, E.R.; Jin, S.; Ramezani, B. Design and optimum energy management of a hybrid renewable energy system based on efficient various hydrogen production. Int. J. Hydrogen Energy 2020, 45, 30113–30128.